

## Flexural performance of FRP-reinforced concrete encased steel composite beams

Ilker Fatih Kara\*

Civil Engineering Department, Bursa Technical University, 152 Evler Mahallesi Eğitim Caddesi,  
1. Damla Sok. No: 2/10, 16330, Bursa, Turkey

(Received November 30, 2015, Revised June 17, 2016, Accepted June 24, 2016)

**Abstract.** This paper presents a numerical method for estimating the curvature, deflection and moment capacity of FRP-reinforced concrete encased steel composite beams (FRP-RCS). A sectional analysis is first carried out to predict the moment-curvature relationship from which beam deflection and moment capacity are then calculated. Comparisons between theoretical and experimental results of tests conducted elsewhere show that the proposed numerical technique can accurately predict moment capacity and deflection of FRP-RCS composite beam. The numerical results also indicated that beam ductility and stiffness are improved when encased steel is added to FRP reinforced concrete beams. ACI, ISIS and Bischoff models for deflection prediction compared well at low load, however, significantly underestimated the experimental results for high load levels.

**Keywords:** fiber reinforced polymers; deflection; ductility; concrete; encased steel beam

---

### 1. Introduction

Corrosion of steel reinforcement constitutes one of the major problems that shorten the lifetime serviceability of concrete structures. Many steel-reinforced concrete structures exposed to deicing salts and marine environments require extensive and expensive maintenance to minimize the effect of steel reinforcement corrosion. Recently, fiber reinforced polymer (FRP) bars have been adopted as a potential solution to the corrosion problems in concrete structures. In addition to the noncorrosive nature of FRP materials, they also have a high strength-to-weight ratio that makes them attractive as reinforcement for concrete structures. However, due to the low elastic modulus of FRP bars, concrete beams reinforced with FRP show larger deflections and wider cracks than counterpart steel-reinforced concrete beams with the same cross section and reinforcement area. Hence, FRP reinforced concrete design is generally controlled by serviceability limit states. Moreover, the elasticity of FRP bars is linear up to failure and the flexural failure mode of FRP-reinforced concrete beams is brittle rather than ductile. Design codes encourage over-reinforced FRP design since it is more progressive and leads to a less catastrophic failure with a higher degree of deformability. However, it can not be applied to cases such as seismic application where the internal force redistribution is very important (Li *et al.* 2012, Gholami *et al.* 2016).

---

\*Corresponding author, Ph.D., E-mail: [ilker.kara@btu.edu.tr](mailto:ilker.kara@btu.edu.tr)

An improvement of the structural performances of concrete beams can be obtained by using a combination of FRP and steel reinforcements or, alternatively, FRP rebars manufactured combining two or more different reinforcing fibers (hybrid FRP rebars). The concept of using a hybrid composite by combining two or more different reinforcing fibers to produce a bilinear stress-strain behavior has been a subject of interest. The hybrid FRP rebars consisting of more than one reinforcing material behave in an elastic-pseudo ductile manner due to the fact that the reinforcing fibers such as glass, aramid, carbon fibers and steel core have different stiffness and ultimate strains. The researches (Cheung and Tsang 2010, Etman 2011, Harris *et al.* 1998, Nanni *et al.* 1994, Wu *et al.* 2012) indicated that the flexural capacity and ductility of FRP-RC members can be increased by using the hybrid FRP bars. However, such efforts have thus far resulted in limited practical developments. Recently, the effect of the arrangement of FRP bars and steel bars on the durability of concrete members has been investigated experimentally and theoretically (Aiello and Ombres 2002, Lau and Pam 2010, Leung and Balendran 2003, Mohamed 2013, Tan 1997, Wenjun *et al.* 2009). It was found that placing FRP rebars near the outer surface of the tensile zone with small cover thickness values and steel rebars at the inner level of the tensile zone provides an optimal solution for the durability of concrete beams. The experimental studies also indicated that a combination of FRP and steel reinforcement provides improved serviceability and ductility compared to FRP reinforced concrete beams. Furthermore, the theoretical study from recent work (El-Helou and Aboutaha 2015) on hybrid steel-GFRP reinforced concrete beam columns concluded that hybrid steel-GFRP composite concrete sections show adequate ductility with a significant increase in strength. Meanwhile, a number of research studies (Dundar *et al.* 2008, El-Tawil and Deierlein 1999, Ricles and Paboojian 1994, Weng 2002) on concrete encased steel members validated their desirable ductility and energy-dissipating capacity for seismic application. More recently, the experimental research has been conducted on the flexural behaviour of FRP-RC members with encased structural steel shapes (Li *et al.* 2012). This study showed that using encased steel shapes can provide a significant enhancement in load carrying capacity, stiffness, ductility and energy absorption capacity of tested beams. The experimental results also indicated that concrete compressive strength had insignificant effect on the load carrying capacity of FRP-RCS beams. To the knowledge of the author, no any other study in the past has been carried out to investigate the flexural behaviour of FRP-RC members with encased structural steel shapes.

In the present study, a numerical technique has been developed to predict the moment-curvature relationship and, hence, moment capacity and deflections of FRP-RCS composite beam. In the proposed procedure, a sectional analysis is carried out, where the cross-section of composite beam is divided into a number of concrete and encased steel segment. The member deflection is then obtained from the moment-curvature relationship. A parametric study was carried out to study the effect of the type and amount of FRP reinforcement and encased steel on the moment-curvature relationship and moment capacity of FRP-RCS beams. The present study has also evaluated ACI, ISIS and Bischoff's equation available in the literature for deflection predictions against the experimental results of FRP reinforced concrete beams with encased steel shapes. The proposed procedure would contribute to future studies of FRP-RCS composite beams.

## 2. Numerical approach

An iterative numerical method for predicting the curvature, deflection and moment capacity of

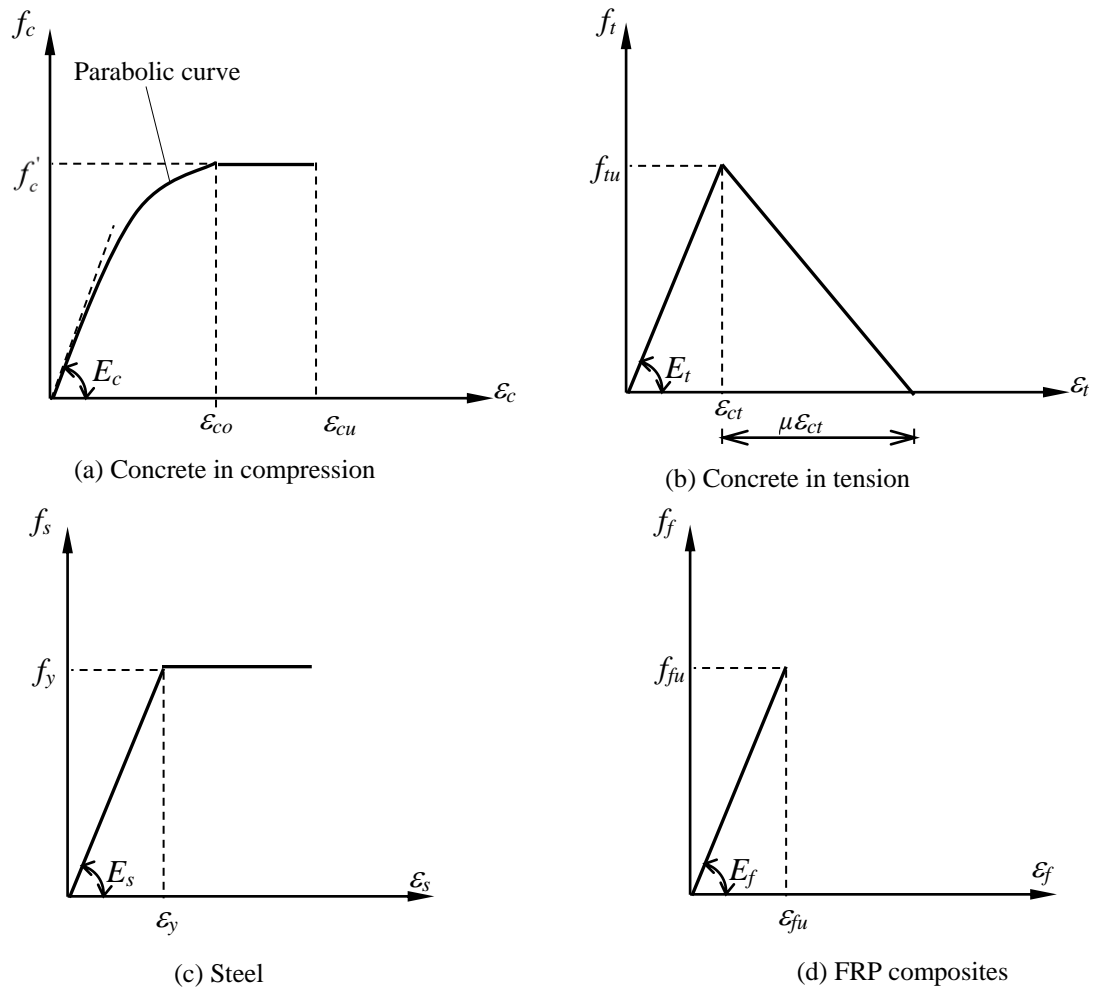


Fig. 1 FRP, steel and concrete stress-strain relationships

FRP-RCS composite beam is presented. Force equilibrium and strain compatibility equations for a beam section divided into a number of segments are numerically solved due to the non-linear behaviour of concrete and steel. The beam deflection is then calculated from the mid-span curvature. The following section describes the process in greater detail.

### 2.1 Constitutive laws of the materials

The stress-strain relationships of concrete, encased steel and FRP reinforcements implemented in this investigation are shown in Fig. 1. However, the numerical technique proposed can accommodate other material models. CEB-FIP (1990) model is adopted for concrete stress-strain relationship in compression as shown in Fig. 1(a). This model can be represented by the following equations

$$f_c = f_c' \left( \frac{2\varepsilon_c}{\varepsilon_{co}} - \left( \frac{\varepsilon_c}{\varepsilon_{co}} \right)^2 \right) \quad \varepsilon_c < \varepsilon_{co} \quad (1a)$$

$$f_c = f_c' \quad \varepsilon_{co} \leq \varepsilon_c \leq \varepsilon_{cu} \quad (1b)$$

where  $f_c$  and  $\varepsilon_c$  are the compressive stress and strain in concrete, respectively,  $f_c'$  is the cylinder compressive strength of concrete,  $\varepsilon_{co}$  ( $=0.002$ ) is the strain in concrete at maximum stress and  $\varepsilon_{cu}$  ( $=0.0035$ ) is the ultimate strain of concrete as shown in Fig. 1(a).

A bi-linear stress-strain relationship is adopted to model concrete in tension as shown in Fig. 1(b) and given below

$$f_t = E_t \varepsilon_t \quad \varepsilon_t \leq \varepsilon_{ct} \quad (2a)$$

$$f_t = f_{tu} - \frac{f_{tu}}{\mu \varepsilon_{ct}} (\varepsilon_t - \varepsilon_{ct}) \quad \varepsilon_{ct}(1 + \mu) \geq \varepsilon_t > \varepsilon_{ct} \quad (2b)$$

where  $f_t$  and  $\varepsilon_t$  are the tensile stress and strain in concrete, respectively,  $f_{tu}$  ( $=0.62\sqrt{f_c'}$ ) and  $\varepsilon_{ct}$  are the tensile strength and corresponding tensile strain of concrete, respectively,  $E_t$  is the tensile modulus of concrete, assumed to be the same as  $E_c$ , and  $\mu$  is a factor controlling the rate of tensile strength decay.

Encased steel is modelled as an elastic-plastic material with yield stress  $f_y$ , as shown in Fig. 1(c). The stress-strain relationship of FRP bars is linear elastic up to rupture and given by

$$f_f = E_f \varepsilon_f \quad \varepsilon_f \leq \varepsilon_{fu} \quad (3)$$

where  $f_f$  and  $\varepsilon_f$  are the stress and strain in FRP bars, respectively,  $E_f$  is the modulus of elasticity of FRP bars, and  $f_{fu}$  and  $\varepsilon_{fu}$  are the ultimate strength and strain of FRP bars, respectively, as shown in Fig. 1(d).

## 2.2 Moment-curvature relationship of composite concrete sections

The composite beam cross section is divided into a number of concrete segments,  $n$ , and web section of encased steel segments,  $m$ , to accommodate the nonlinear stress-strain relationships of concrete and steel in the analysis. For a particular curvature value, strains in each concrete segment and web sections of encased steel segment are determined. In addition, the strains in tensile and compressive FRP bars; and top and bottom encased steel flange are computed. The stresses in each material are, hence, obtained from the respective stress-strain relationships. Equilibrium of forces and moments are eventually considered as explained below.

The iterative numerical procedure starts by assuming a small value of strain at the concrete extreme compression fiber. For each strain  $\varepsilon_c$  at the top level of concrete section, the neutral axis depth,  $x$ , is initially assumed and the correct value is iteratively obtained when equilibrium of forces is satisfied. According to the assumption that plane section before bending remains plane after bending, the strain in each concrete and web section of steel segment are linearly proportional to its distance from the neutral axis (Fig. 2) as expressed below

$$\varepsilon_i = \frac{x - x_i}{x} \varepsilon_c \quad (4a)$$

$$\varepsilon_{swj} = \frac{x - x_j}{x} \varepsilon_c \quad (4b)$$

where  $\varepsilon_c$  is the strain at the top compression level of the reinforced concrete section;  $\varepsilon_i$  is the concrete compressive or tensile strain at mid-depth of  $i$ -th segment, and  $\varepsilon_{swj}$  is the compressive or tensile strain in the web section of encased steel at mid-depth of  $j$ -th segment.

Assuming perfect bond between concrete and FRP bars, and strain compatibility, strains in tensile and compressive FRP bars can be obtained from

$$\varepsilon'_f = \frac{x - d'_f}{x} \varepsilon_c \quad (5)$$

$$\varepsilon_f = \frac{x - d_f}{x} \varepsilon_c \quad (6)$$

where  $\varepsilon_f$  and  $\varepsilon'_f$  indicate the strains in bottom and top reinforcing FRP bars,  $d_f$  and  $d'_f$  are the bottom and top FRP reinforcement depths, respectively.

The strains in top and bottom encased steel flange can also be determined using the same assumption, i.e., perfect bond between concrete and encased steel, as follows.

$$\varepsilon_{stf} = \frac{x - d_{st}}{x} \varepsilon_c \quad (7)$$

$$\varepsilon_{sbf} = \frac{x - d_{sb}}{x} \varepsilon_c \quad (8)$$

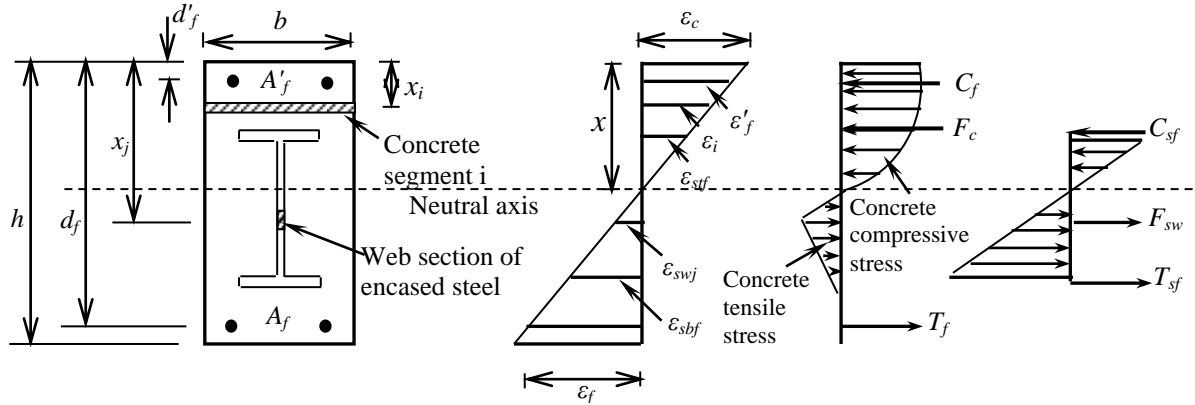
where  $\varepsilon_{stf}$  and  $\varepsilon_{sbf}$  are the strain in center of top and bottom flange of encased steel, and  $d_{st}$  and  $d_{sb}$  are the distance from the top surface of composite beams to center of top and bottom flange of encased steel, respectively.

The corresponding stresses in each concrete and web section of encased steel segment, and top and bottom flange of encased steel and FRP reinforcements can be calculated from the respective stress-strain relationships of concrete, steel and FRP bar presented in Fig. 1. The total concrete force including the contribution of compressive and tensile forces is calculated using Eq. (9) below

$$F_c = \sum_{i=1}^n f_{ci} h_i b \quad (9)$$

where  $f_{ci}$  is the concrete compressive or tensile stress at the centroid of the  $i$ -th segment,  $h_i$  ( $=h/n$ ) is the thickness of the  $i$ -th segment,  $n$  is the total number of section segments,  $h$  is the beam depth and  $b$  is the beam width. This summation extends over all compressive and tensile concrete segments. The total force for web section of encased steel containing the contribution of compressive and tensile forces is computed as follows

$$F_{sw} = \sum_{j=1}^m \sigma_{sj} d_j t_w \quad (10)$$



(a) FRP-RCS composite concrete section (b) Strain distribution (c) Stress distribution and forces

Fig. 2 Strains, stresses and forces of composite concrete section

where  $\sigma_{sj}$  is the steel compressive or tensile stress for web section at the centroid of the  $j$ -th segment,  $d_j (=d/m)$  is the thickness of the  $j$ -th segment,  $m$  is the total number of steel web section segments,  $d$  and  $t_w$  are the depth and thickness of encased steel web section, respectively. The forces in top and bottom encased steel flange and FRP bars are estimated from

$$T_{sf} = A_{stf} E_s \varepsilon_{stf} \quad (11)$$

$$C_{sf} = A_{sbf} E_s \varepsilon_{sbf} \quad (12)$$

$$T_f = A_f E_f \varepsilon_f \quad (13)$$

$$C_f = A'_f E'_f \varepsilon'_f \quad (14)$$

$T_{sf}$ , and  $A_{sbf}$  are the force and area of bottom encased steel flange and  $C_{sf}$ , and  $A_{stf}$  are the corresponding values of top encased steel flange. In the same equations,  $E_s$  is the modulus of elasticity of encased steel. In Eqs. (13) and (14),  $T_f$ ,  $A_f$  and  $E_f$  are the force, area, and modulus of elasticity of bottom reinforcing FRP bars, respectively,  $C_f$ ,  $A'_f$  and  $E'_f$  are the corresponding values of top FRP reinforcement. Eqs. (13) and (14) are also valid for different types of FRP bars, i.e., GFRP, AFRP and CFRP, provided that the appropriate modulus of elasticity,  $E_f$ , and tensile rupture,  $f_{fu}$ , are used. Considering equilibrium of forces, the following equation is obtained

$$F_c + C_{sf} + C_f = T_f + T_{sf} + F_{sw} \quad (15a)$$

$$\sum_{i=1}^n f_{ci} h_i b + A'_f E'_f \varepsilon'_f + A_{stf} E_s \varepsilon_{stf} = A_f E_f \varepsilon_f + A_{sbf} E_s \varepsilon_{sbf} + \sum_{j=1}^m \sigma_{sj} d_j t_w \quad (15b)$$

In the above Eq. (15), the neutral axis depth  $x$  is the only unknown. The value of  $x$  is iteratively adjusted using the bi-section method until sufficient equilibrium accuracy is attained, for example

$$\frac{|F_c + C_{sf} + C_f - T_f - T_{sf} - F_{sw}|}{|F_c|} \leq 10^{-8} \quad (16)$$

The beam curvature  $\varphi$  can also be determined from the strain distribution as follows (see Fig. 2(b))

$$\varphi = \frac{\varepsilon_c}{x} \quad (17)$$

The applied moment  $M_{fs}$  of the composite section is then calculated by taking moments of internal forces about any horizontal axis, for instance about the neutral axis

$$M_{fs} = \sum_{i=1}^n F_{ci}(x - x_i) + \sum_{j=1}^m F_{sw}(x - x_j) + T_f(x - d_f) + T_{sf}(x - d_{sbf}) + C_f(x - d'_f) + C_{sf}(x - d'_{stf}) \quad (18)$$

where  $F_{ci}$  ( $=f_{ci}h_i b$ ) is the concrete compressive or tensile force at the centroid of the  $i$ -th segment;  $F_{sw}$  ( $=\sigma_{sj} d_j t_w$ ) is the steel compressive or tensile stress for web section at the centroid of the  $j$ -th segment.

The strain in the extreme concrete compression fibre is incrementally increased and the above procedure is repeated for each value of strain until the maximum concrete compressive strain reaches its ultimate compressive strain ( $\varepsilon_{cu}=0.0035$ ). During such strain increase until concrete crushing, rupture of FRP bars or yielding of (bottom flange of) encased steel may occur depending on the amount of FRP/encased steel in the section. The section moment capacity  $M_{fs}$  is, therefore, the highest moment attained for various increments considered until failure. Based on the aforementioned procedure, a computer program has been developed for the moment-curvature relationship and moment capacity of FRP-RC sections with encased structural steel shapes.

### 2.3 Failure modes of FRP-RCS composite beams

For concrete beams reinforced with either steel or FRP, the balanced reinforcement ratio is attained when the beam fails by crushing of concrete in compression and either yielding of steel or rupture of FRP in tension, simultaneously. However, a failure condition of FRP-RCS composite beams, in which crushing of concrete, yielding of tensile flange of encased steel and rupture of FRP simultaneously take place, is almost impossible to occur in practice. In practice, the tensile flange of encased steel would have yielded long before rupture of FRP reinforcement as the steel yield strain ( $\varepsilon_y \sim 0.0015$ ) is far much less than the FRP rupture strain ( $\varepsilon_f \sim 0.01$ ). Hence, the balanced condition for FRP-RCS composite beams is proposed in a way such that concrete crushing in compression and rupture of FRP reinforcement simultaneously occur, while tensile flange of encased steel has already yielded. Five types of possible flexural failures (FRP fracture failure; crushing of concrete- rupture of FRP simultaneously; steel yielding followed by concrete crushing failure; crushing of concrete- steel yielding simultaneously and over-reinforced failure (crushing of concrete before yielding of steel)) of an FRP-RCS beam can be expected depending on the ratio and configuration of encased steel and amount of FRP reinforcement. On the other hand, for an FRP-RCS beam with a ratio of encased steel area to gross cross-sectional area not less than 0.02 that is recommended by the Chinese code (Chen *et al.* 1999) for conventional concrete encased steel members, its failure generally starts by steel yielding followed by concrete crushing and lastly by FRP rupture. This failure mode is similar to the under-reinforced of conventional case, and is the most desired failure mode to ensure the ductility of FRP-RCS beams and provide the effective use of each material in the composite section.

Table 1 Details of FRP-RCS composite beams tested in the literature.

| Beam notation | Width (mm) | Overall depth (mm) | Span (mm) | $f_{cu}$ (MPa) | $A_f$                  | $A'_f$                | $E_f$ (kN/mm <sup>2</sup> ) | Encased steel shape<br>$b_f \times d_s \times t_f \times t_w$ |
|---------------|------------|--------------------|-----------|----------------|------------------------|-----------------------|-----------------------------|---|
| B2            | 160        | 250                | 2000      | 48.2           | 3 $\Phi$ 12            | 2 $\Phi$ 6            | 38                          | 80×140×9.1×5.5  |
| B3            | 160        | 250                | 2000      | 48.2           | 2 $\Phi$ 12            | 2 $\Phi$ 6            | 38                          | 80×140×9.1×5.5  |
| B4            | 160        | 250                | 2000      | 35.5           | 2 $\Phi$ 8             | 2 $\Phi$ 6            | 38                          | 80×140×9.1×5.5  |
| B5            | 160        | 250                | 2000      | 35.5           | 3 $\Phi$ 12            | 2 $\Phi$ 6            | 38                          | 80×140×9.1×5.5  |
| B6            | 160        | 300                | 2000      | 48.2           | 3 $\Phi$ 12+2 $\Phi$ 6 | 2 $\Phi$ 6            | 38                          | 80×140×9.1×5.5  |
| B7            | 160        | 300                | 2000      | 48.2           | 2 $\Phi$ 8             | 2 $\Phi$ 12+ $\Phi$ 8 | 38                          | 80×140×9.1×5.5  |

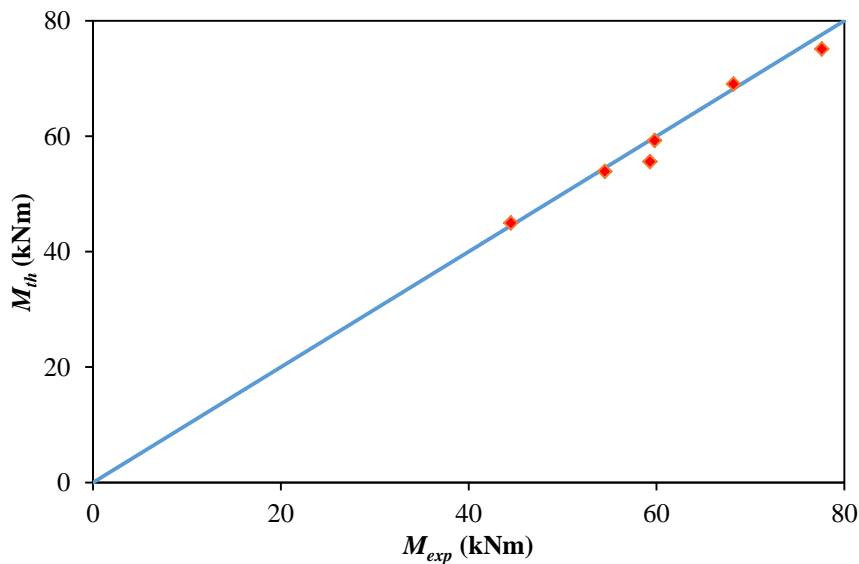
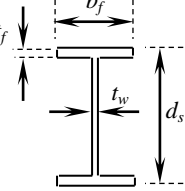


Fig. 3 Experimental versus predicted moment capacities of FRP-RCS composite beams

#### 2.4 Validation of the proposed numerical model

Test results of six FRP-RCS composite beams collected from previous experimental investigation in the literature (Li *et al.* 2012) are used to validate the proposed numerical method. Table 1 lists the geometrical and material properties of all beams considered. All the six beams were reported to have failed in flexure; steel yielding following by concrete crushing failure modes. Comparisons between predictions from the current numerical technique and flexural moment capacities of all FRP-RCS composite beams collected are presented in Table 2 and Fig. 3. The average and standard deviation of the ratio between the present technique and experimental bending capacities,  $M_{th}/M_{exp}$ , are 0.98 and 2.8%, respectively. The ratio of  $M_{th}/M_{exp}$  varies between 0.94 and 1.01. Overall, the predictions obtained from the current analysis are in good agreement with the experimental results. The failure modes are also correctly predicted by the present technique for six composite beams considered as reported in Table 2.

Table 2 Comparisons between the theoretical and experimental flexural moment capacities of FRP-RCS composite beams tested in the literature

| Beam notation                | $M_{exp}$ (kNm) | $M_{the}$ (kNm) | $M_{the}/M_{exp}$ | Experimental mode of failure |
|------------------------------|-----------------|-----------------|-------------------|------------------------------|
| B2                           | 59.8            | 59.3            | 0.99              | SY-CC                        |
| B3                           | 54.5            | 53.9            | 0.99              | SY-CC                        |
| B4                           | 44.5            | 45              | 1.01              | SY-CC                        |
| B5                           | 59.3            | 55.6            | 0.94              | SY-CC                        |
| B6                           | 68.2            | 69              | 1.01              | SY-CC                        |
| B7                           | 77.6            | 75.1            | 0.97              | SY-CC                        |
| Average                      |                 |                 | 0.98              |                              |
| Standard deviation (%)       |                 |                 | 2.4%              |                              |
| Coefficient of variation (%) |                 |                 | 2.5%              |                              |

Note:  $M_{exp}$  and  $M_{the}$  are the experimental and theoretical moment capacities of FRP-RCS composite beam sections. Experimental failure mode: SY-CC refers to steel yielding followed by concrete crushing.

### 3. Effect of different parameters on the moment curvature relationship

The proposed numerical technique has been employed to study the effect of the type and amount of FRP reinforcement and configuration of encased steel on the moment-curvature relationship as presented in the following sections.

#### 3.1 Effect of the amount of FRP reinforcement on the moment curvature relationship

The influence of the amount of FRP bars was examined by comparing the moment curvature relationships of FRP-RCS composite sections as predicted in Fig. 4. The dimensions, concrete and encased steel properties are the same for all beams considered in Fig. 4;  $b=180$  mm,  $h=250$  mm,  $f_c'=40$  N/mm<sup>2</sup>,  $E_f=38$  kN/mm<sup>2</sup>,  $f_{fu}=680$  N/mm<sup>2</sup>,  $A'_f=100.48$  mm<sup>2</sup> and  $f_y=273$  N/mm<sup>2</sup>. The limiting case of pure FRP reinforced concrete section are also presented in Fig. 4 against which the behavior of FRP- RCS composite sections may be assessed. The failure in all FRP-RCS composite beams considered starts by steel yielding followed by concrete crushing, before rupture of FRP bars. The amount of FRP reinforcement in pure FRP reinforced concrete beams was also selected in such that the failure mode and ultimate moment capacity of this beam is similar to that of FRP-RCS beams.

It can be observed from Fig. 4 that the initial linear stiffness is similar for all beams studied. The end of the linear phase is identified by concrete cracking and, consequently, FRP bars and encased steel play a more significant role in controlling the beam stiffness depending on the amount of FRP reinforcement. After cracking, the moment-curvature relationship has a less gradient than the initial linear part owing to the decrease in the beam stiffness. The reduction in stiffness due to cracking is almost the same in the composite beams having different amount of FRP reinforcement. On the other hand, as expected the stiffness reduction in pure FRP concrete section is higher than the FRP-RC composite sections. The end of the second part of moment curvature relationships marked the yielding of tensile steel flange, and was followed by a softer slope until (FRP rupture or) concrete crushing. In this phase, FRP reinforcement showed a more

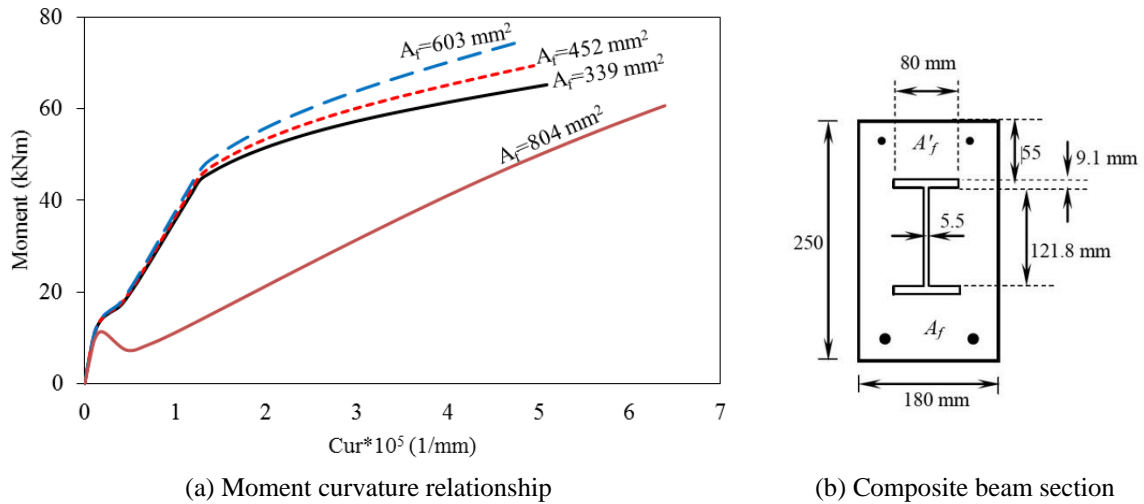


Fig. 4 Effect of amount of FRP reinforcement on the moment curvature relationships of FRP-RCS beam sections

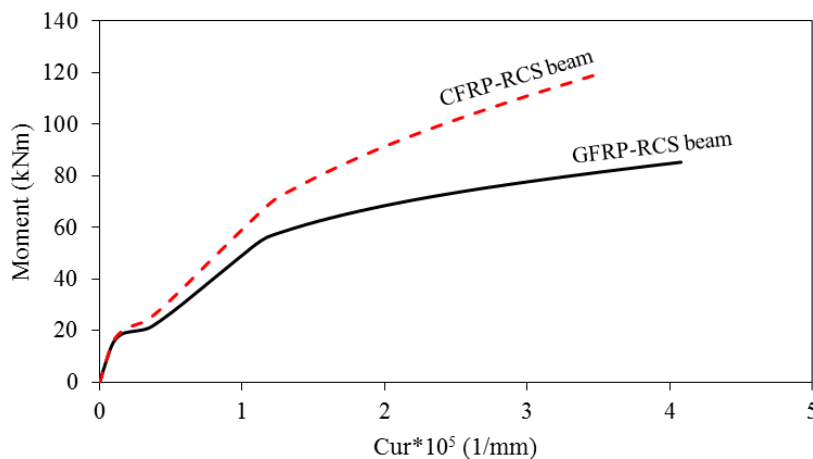


Fig. 5 Effect of type of FRP reinforcement (GFRP or CFRP) on the moment curvature relationships of FRP-RCS composite beam sections

influential role in resisting loads after yielding of tensile steel flange. As seen in Fig. 4(a), the beam stiffness increases with the increase of FRP reinforcement after the steel yielding; the higher the value of  $A_f$ , the higher the stiffness. The results show that increasing the FRP reinforcement was ineffective in enhancing the concrete cracking and steel yielding loads.

### 3.2 Effect of the type of FRP reinforcement on the moment curvature relationship

The current numerical method has also been employed to study the effect of type of FRP reinforcement (glass fiber reinforced polymer (GFRP) or carbon fiber reinforced polymer (CRFP)) on the moment-curvature relationship of FRP-RC composite beams as depicted in Fig. 5. The

dimensions, concrete properties and ratio and configuration of encased steel shapes and amount of FRP reinforcement in each case are the same for all sections considered in Fig. 5;  $b=180$  mm,  $h=300$  mm,  $f_c'=35$  N/mm<sup>2</sup>,  $f_y=273$  N/mm<sup>2</sup>;  $f_{fu}=680$  N/mm<sup>2</sup> and  $E_f=38$  kN/mm<sup>2</sup> for GFRP and  $f_{fu}=1200$  N/mm<sup>2</sup> and  $E_f=120$  kN/mm<sup>2</sup> for CFRP bars. Fig. 5 indicates that GFRP-RCS composite section exhibit a significant reduction in stiffness after yielding of steel in comparison with CFRP-RCS composite section. This behavior is mainly attributed to the lower elastic modulus of GFRP bars than that of CFRP bars leading to a reduced effective moment of inertia and hence larger curvature.

### 3.3 Effect of the ratio and configuration of encased steel

The present numerical technique has also been employed to study the effect of the ratio and configuration of the encased steel shapes on the moment-curvature relationship as presented in Figs. 6 and 7: Fig. 6 shows the influence of the ratio of encased steel whereas Fig. 7 presents the effect of the configuration of encased steel shapes. The dimensions, concrete and encased steel properties and amount of FRP reinforcement are the same for all beams shown in Fig. 6;  $b=180$  mm,  $h=300$  mm,  $f_c'=40$  N/mm<sup>2</sup>,  $E_f=38$  kN/mm<sup>2</sup>,  $f_{fu}=680$  N/mm<sup>2</sup>,  $A_f=452$  mm<sup>2</sup> and  $f_y=273$  N/mm<sup>2</sup>. However, the only parameters changed were the ratio of symmetrically embedded encased steel and configuration of eccentrically embedded encased steel shapes as depicted in Figs. 6 and 7. It can be observed from Fig. 6 that the beams having different ratio of encased steel exhibited similar moment-curvature behavior. The numerical results show that the steel yielding load increases with the increase in the ratio of encased steel. In addition, increasing the ratio of encased steel leads to the increase in the beam stiffness after concrete cracking. The effect of the eccentricity of encased steel on the moment curvature relationships of composite beams is shown in Fig. 7. This Fig. indicates that the increase in the eccentricity of encased steel gives rise to the increase in the moment capacity and steel yielding loads. This may be attributed to the increase of moment arm and tensile stress of encased steel. The higher eccentricity of encased steel leads to higher moment

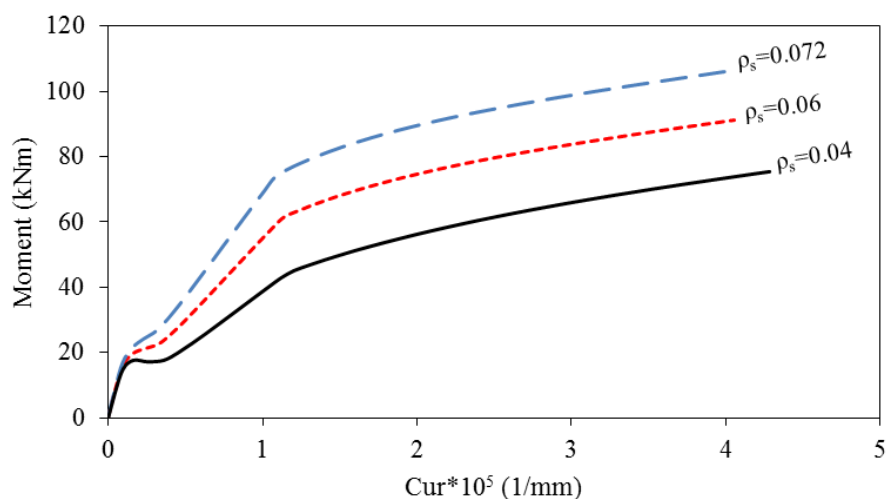
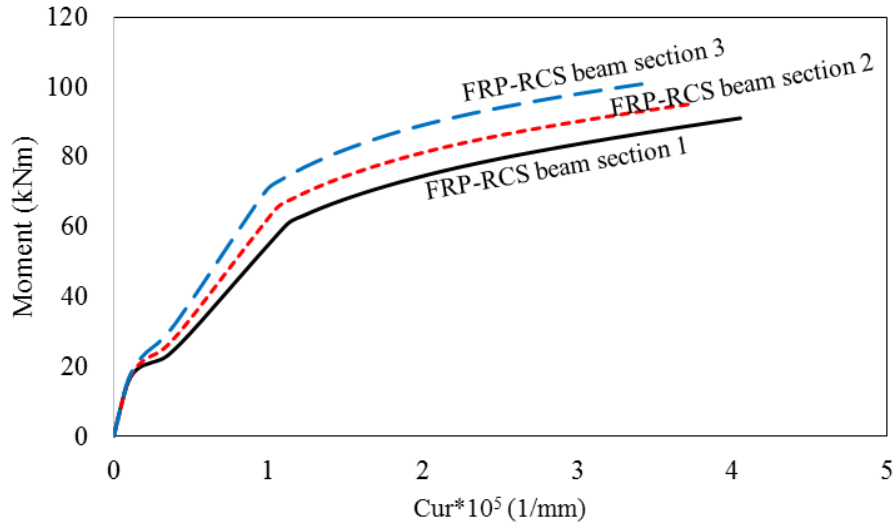
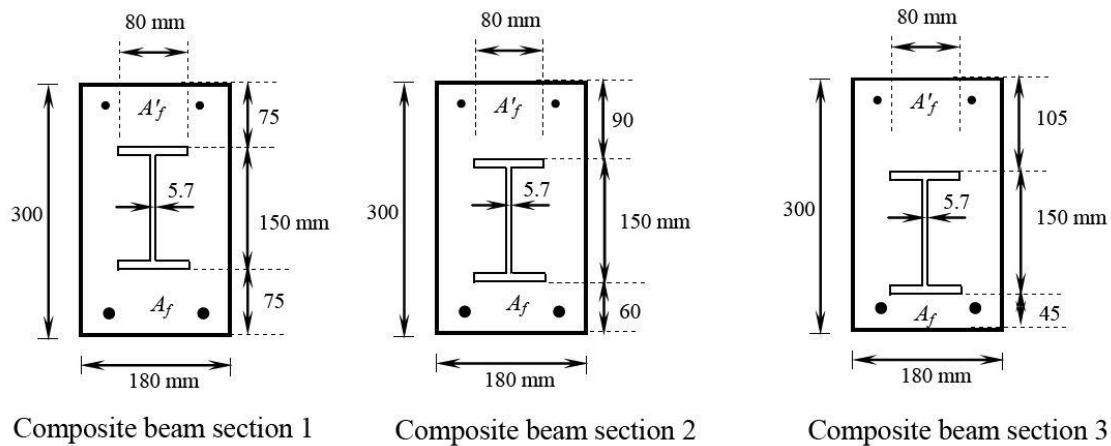


Fig. 6 Effect of ratio of encased steel on the moment curvature relationships of FRP-RCS composite beam sections



(a) Moment-curvature relationship



(b) FRP-RCS composite beam sections considered

Fig. 7 (a-b) Effect of configuration of encased steel on the moment curvature relationships of FRP-RCS composite beam sections

arm and tensile force of encased steel, and, thus increasing the moment capacity of the composite section.

#### 4. Deflection predictions

In this section, a simplified method for deflection calculation of FRP-RCS composite beams is developed from the moment-curvature relationship presented above. The effective flexural rigidity,  $EI_{eff}$ , of the member at the location of the maximum moment is firstly determined from the moment-curvature relationship at each loading as

$$EI_{eff} = \frac{M}{\phi} \quad (19)$$

The midspan deflection,  $\Delta$ , of composite beams is then calculated using the elastic deflection formula, for example, the immediate deflection of simply supported beams loaded with two-point loads, each  $P/2$ , could be also computed from Eq. (20) as follows

$$\Delta = \frac{(Pa/2)(3L^2 - 4a^2)}{24EI_{eff}} \quad (20)$$

where  $a$  is the shear span and  $L$  is the beam span length. The applicability of different models available in the literature for deflection calculations of FRP reinforced concrete beams to FRP-RCS beams is also evaluated by comparing their predictions against the experimental results as well as the current numerical technique.

The ACI Committee 440-06 (2006) provides a modified version of Branson's equation that includes a reduction coefficient,  $\beta_d$ , related to the reduced tension stiffening exhibited by FRP reinforced concrete members as follows

$$I_{eff} = \left(\frac{M_{cr}}{M}\right)^3 \beta_d I_1 + \left[1 - \left(\frac{M_{cr}}{M}\right)^3\right] I_2 \quad (21)$$

$$\beta_d = 0.2 \left(\frac{\rho_f}{\rho_{fb}}\right) \quad (22)$$

where  $I_1$  and  $I_2$  are the moments of inertia of the gross and cracked transformed concrete sections considering the contribution of encased steel and FRP reinforcement to the stiffness, respectively,  $M$  is the applied bending moment,  $M_{cr}$  is the flexural cracking moment,  $\beta_d$  is a reduction coefficient given by Eq. (22),  $\rho_f (=A_f/bd)$  is the FRP reinforcement ratio,  $A_f$  is the area of tensile FRP reinforcement,  $b$  and  $d$  are width and effective depth of FRP reinforced concrete beams and  $\rho_{fb}$  is the balanced FRP reinforcement ratio.

ISIS Canadian network design manual (2002) suggested that the effective moment  $I_{eff}$  of inertia for deflection calculations of FRP reinforced concrete members can be taken as

$$I_{eff} = \left( \frac{I_1 I_2}{I_1 + \left(1 - 0.5 \left(\frac{M_{cr}}{M}\right)^2 (I_1 - I_2)\right)} \right) \quad (23)$$

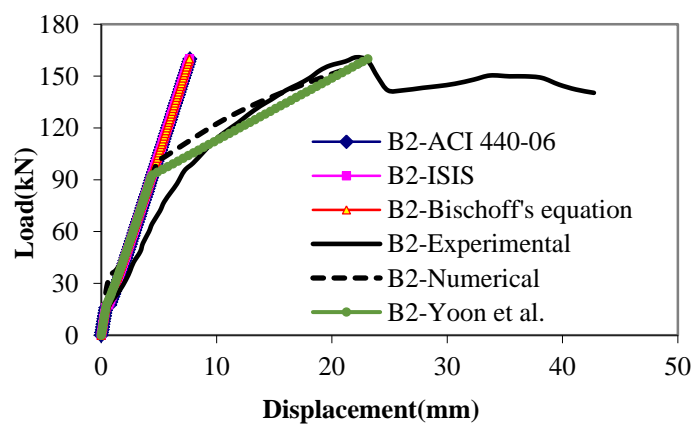
On the other hand, Bischoff (2007) recommended the following expression related to an equivalent moment of inertia based on the tension-stiffening effect on curvature

$$I_{eff} = \left( \frac{I_2}{1 - \left(1 - \frac{I_2}{I_1}\right) \left(\frac{M_{cr}}{M}\right)^2} \right) \quad (24)$$

However, because the deflection behavior of the FRP-RCS composite beams changes especially after the yielding of steel, the method suggested by Yoon *et al.* (2011) to predict the deflection after steel yielding of hybrid reinforced beams was also adopted for FRP-RCS composite beams. Yoon *et al.* (2011) suggested the following the effective moment  $I_{eff}$  of inertia equation after steel yielding based on Bischoff's approach for deflection calculations of hybrid reinforced beams with steel bars

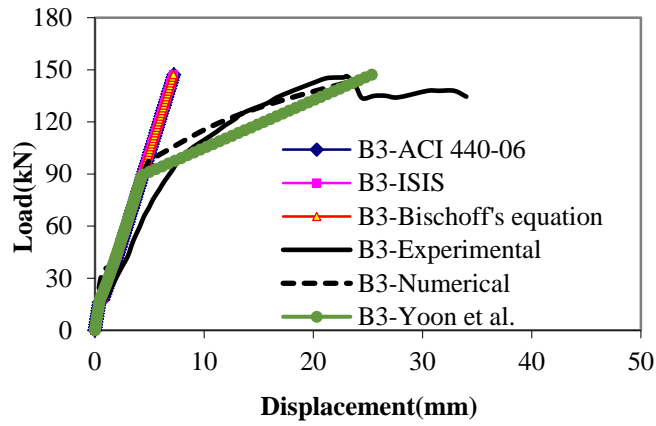
$$I_{eff} = \left( \frac{I_2}{\frac{I_2}{I_y} + \frac{M_y}{M} \left( 1 - \frac{I_2}{I_y} \right) - \left( 1 - \frac{I_2}{I_1} \right) \left( \frac{M_{cr}}{M} \right)^2} \right) \quad (25)$$

where  $M_y$  is the steel yielding moment and  $I_y$  is the moment of inertia after steel yields. It should be expressed that the effective moment of inertia ( $I_{eff}$ ) proposed by Bischoff (2007) is used before steel yielding while using the method suggested by Yoon *et al.* (2011) in the deflection calculation. The mid-span experimental deflections of composite beams tested by Li *et al.* (2012) are compared with the predictions from the current numerical technique and other models in Eqs. (21) to (25); see Fig. 8(a)-(f). The geometrical dimensions, reinforcement details and material properties of beams considered are given in Table 1. The deflection results obtained from the present numerical technique agree well with the test results. Fig. 8 indicates that the present technique is able to predict both the pre and post cracking deflections and to capture the beam stiffness and deflection after yielding of steel. Fig. 8 also shows that the deflections predicted by different models compare well at low load levels before and after the first cracking load. However, the predictions of ACI, ISIS and Bischoff's models considered significantly underestimate the experimental results for high load levels. On the other hand the model suggested by Yoon *et al.* predicted the deflections fairly well even after steel yields. Fig. 8 also indicates that deflection results obtained from ACI,

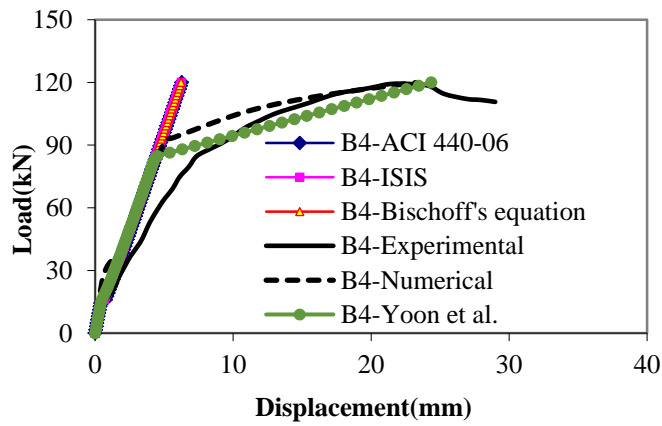


(a)

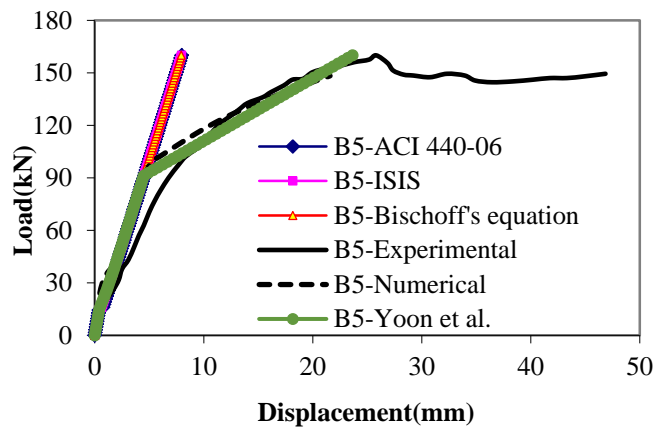
Fig. 8 (a-f) Comparison between experimental and theoretical deflections of FRP-RCS beams tested in the literature



(b)

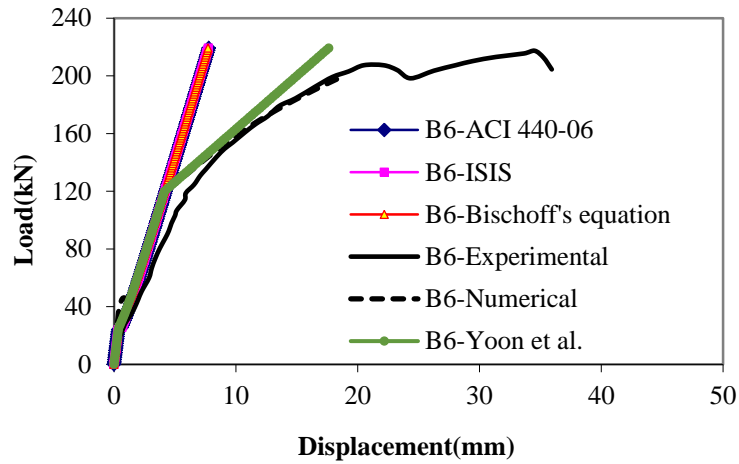


(c)

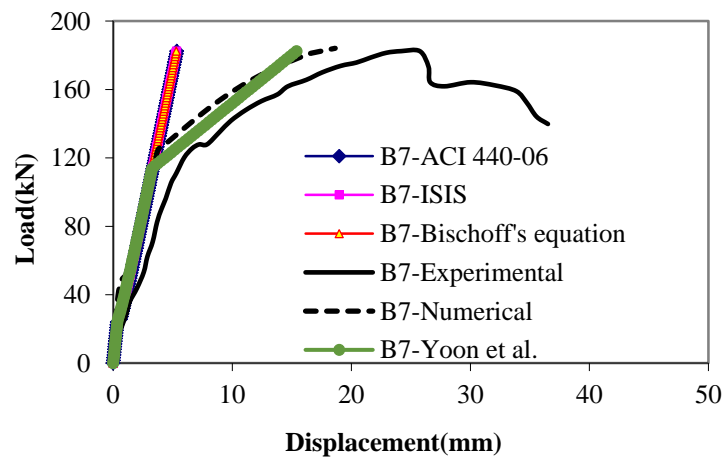


(d)

Fig. 8 Continued



(e)



(f)

Fig. 8 Continued

ISIS and Bischoff's effective moment of inertia models are very close to one another.

Fig. 9 shows the variation of the flexural rigidity,  $EI_{eff}$ , of four FRP-RCS composite beams against the applied moment. The moment-effective flexural rigidity curve consists of different segments, denoting the pre-cracking, post-cracking, yielding of tensile steel flange and concrete crushing stages. In the pre-cracking stage, the composite beams showed the highest flexural stiffness. Once the beams cracked, the flexural rigidity was notably reduced but remained almost constant until yielding of tensile steel. A further reduction of  $EI_{eff}$  is depicted after the yielding of tensile steel flange up to concrete crushing failure.

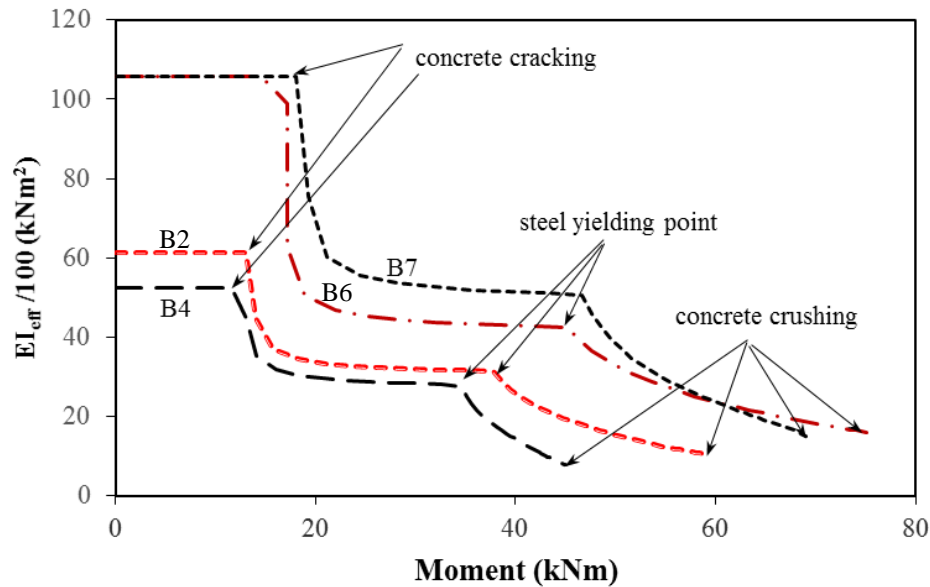


Fig. 9 Effective flexural stiffness variations

#### 4. Conclusions

An iterative numerical method for predicting the flexural behaviour of FRP-RCS composite beams has been presented. The moment-curvature relationship of FRP-RCS beams is numerically obtained by considering force equilibrium and strain compatibility. The beam deflection is then calculated from the mid-span curvature. Comparisons between experimental results available in the literature and moment capacity and deflection of FRP-RCS composite beams show good agreement. The proposed technique is able to predict both the pre and post cracking deflections up to the beam failure and to capture the beam behavior after yielding of encased steel.

The parametric study concluded that the contribution of encased steel to FRP concrete beams provides ductility and stiffness improvement of beams studied. FRP reinforcement was found to play a more influential role in resisting loads after yielding of tensile steel flange. The results also indicated that increasing the FRP reinforcement was ineffective in enhancing the concrete cracking and steel yielding loads.

ACI, ISIS and Bischoff models for deflection prediction compare well at low load levels before and after the first cracking load, however, significantly underestimate the experimental results for high load levels. It should also be noted that these different models provide quite similar results. On the other hand the modified form of Bischoff's equation for the effective moment of inertia including the yielding of encased steel gives the most accurate results of deflections among the existing models considered in this study.

#### References

Aiello, M.A. and Ombres, L. (2002), "Structural performances of concrete beams with hybrid (fiber-

- reinforced polymer-steel) reinforcements”, *J. Compos. Constr.*, **6**(2), 133-140.
- American Concrete Institute (ACI) (2006), “Guide for the design and construction of concrete reinforced with FRP bars”, ACI 440.1R-06, Farmington Hills, MI.
- Bischoff, P.H. (2007), “Deflection calculation of FRP reinforced concrete beams based on modifications to the existing Branson equation”. *J. Compos. Constr.*, **11**(1), 4-14.
- Canadian Standards Association (CSA) (2002), “Design and construction of building components with fibre-reinforced polymers”, CSA Standard S806-02, Rexdale, Ont., Canada.
- CEB-FIP (1990), “Model code for concrete structures, Comite Euro-International du Beton”, Bulletin, 213/214.
- Chen, C.C., Weng, C., Lin, I.M. and Li, J.M. (1999), “Seismic behaviour and strength of concrete encased steel stub columns and beam-columns”, Report No. MOIS 881012-1, Architecture and Building Research Institute. (in Chinese)
- Cheung, M.M.S. and Tsang, T.K.C. (2010), “Behaviour of concrete beams reinforced with hybrid FRP composite rebar”, *Adv. Struct. Eng.*, **13**(1), 81-93.
- Dundar, C., Tokgoz, S., Tanrikulu, A.K. and Baran, T. (2008), “Behavior of reinforced and concrete-encased composite columns subjected to biaxial bending and axial load. Building and Environment”, *Constr. Build. Mater.*, **43**, 1109-20.
- El-Helou, R.G. and Aboutaha, R.S. (2015), “Analysis of rectangular hybrid steel-GFRP reinforced concrete beam columns”, *Comput. Concrete*, **16**(2), 245-260.
- El-Tawil, S. and Deierlein, G.G. (1999), “Strength and ductility of concrete encased composite columns”, *J. Struct. Eng.*, **125**(9), 1009-19.
- Etman, E.E. (2011), “Innovative hybrid reinforcement for flexural members”, *J. Compos. Constr.*, **15**(2), 2-8.
- Gholami, M., Mohd Sam, A.R., Marsono, A.K., Tahir, M.M. and Faridmehr, I. (2016), “Performance of steel beams strengthened with pultruded CFRP plate under various exposures”, *Steel Comp. Struct.*, **20**(5), 999-1022.
- Harris, H.G., Somboonsong, W. and Ko, F.K. (1998), “New ductile hybrid FRP reinforcing bar for concrete structures”, *J. Compos. Constr.*, **2**(1), 28-37.
- Lau, D. and Pam, H.J. (2010), “Experimental study of reinforced concrete beams”, *Eng. Struct.*, **32**, 3857-3865.
- Leung, H.Y. and Balendran, R.V. (2003), “Flexural behaviour of concrete beams internally reinforced with GFRP rods and steel rebars”, *Struct. Surv.*, **21**(4), 146-157.
- Li, X., Lv H. and Zhou S. (2012), “Flexural behavior of GFRP-reinforced concrete encased steel composite beams”, *Constr. Build. Mater.*, **28**, 255-262.
- Mohamed, A.S. (2013), “Flexural behavior and design steel-GFRP reinforced concrete beams”, *ACI Mater. J.*, **10**(6), 677-85.
- Nanni, A., Henneke M.J. and Okamoto, T. (1994), “Behavior of concrete beams with hybrid reinforcement”, *Constr. Build. Mater.*, **8**(2), 89-95.
- Ricles, J.M. and Paboojian, S.D. (1994), “Seismic performance of steel-encased composite columns”, *J. Struct. Eng.*, **120**(8), 2474-2494.
- Tan, K.H. (1997), “Behaviour of hybrid FRP-steel reinforced concrete beams”, *Proc., 3rd Int. Symp. on Non-Metallic (FRP) Reinforcement for Concrete Structures (FRPRCS-3)*, Japan Concrete Institute, Sapporo, 487-494.
- Weng, C.C., Yen, S.I. and Jiang, M.H. (2002), “Experimental study on shear splitting failure of full-scale composite concrete encased steel beams”, *J. Struct. Eng.*, **128**(9), 1186-94.
- Wenjun, Q., Zhang, X. and Huang, H. (2009), “Flexural behavior of concrete beams reinforced with hybrid (GFRP and steel) bars”, *J. Compos. Constr.*, **13**(5), 350-359.
- Wu, G., Sun, Z.Y., Wu, Z.S. and Luo, Y.B. (2012), “Mechanical Properties of Steel-FRP Composite Bars and Performance of SFCB Reinforced Concrete Structures”, *Adv. Struct. Eng.*, **15**(4), 625-635.
- Yoon, Y.S., Yang, J.M., Min, K.H. and Shin, H.O. (2011), “Flexural strength and deflection characteristics of high strength concrete beams with hybrid FRP and steel bar reinforcement”, *10<sup>th</sup> International*

*symposium on fiber-reinforced polymer reinforcement for concrete structures 2011*, FRPRCS-10, Tampa (FL, United States)/38800 Country Club Drive, Farmington Hills, MI 48331, American Concrete Institute, US.

CC